Bubble Mapping: A Novel Approach for Three-Dimensional Visualisation of Gas-Liquid Flow by Electrical Tomography

Qiang Wang[1], Xiaodong Jia[1], Mi Wang[1,*]

School of Chemical and Process Engineering, University of Leeds, Leeds LS2 9JT, UK

Abstract: Due to the relatively low spatial resolution, electrical tomograms of a gas-liquid flow are ineffective in indicating small bubbles or sharp interfaces between large bubbles and the liquid. These limitations give rise to ambiguity in human or machine perception of flow dynamics, e.g. bubble size and bubble distribution. In this paper, a novel approach, called bubble mapping, is proposed for 3D visualisation of gas-liquid flows. With this approach, a stack of cross-sectional tomograms by electrical tomography is transformed and displayed as a collection of individual air bubbles. The result is akin to a photographic imagining of the same flow, thus even to the untrained eyes it is immediately obvious where and how large the bubbles are and what flow regime it is in. The transformation is done with the help of a lookup table indexed by bubble size and distribution and an enhanced isosurface algorithm. This new approach has been applied to a two-phase flow rig and its performance compared with photo images taken from a transparent section of the flow rig by a high-speed camera. Reasonable agreements have been obtained for common flow regimes including bubbly flow, stratified flow, plug flow, slug flow and annular flow. It is well known that electrical tomography is capable of "seeing" through opaque pipe walls and flow media. This ability combined with the bubble mapping means that photorealistic flow visualisation and visual identification of flow regime is now possible for many real industrial applications where pipe walls and flow media are often opaque. It is also worth noting that the bubble mapping approach is designed to be generic and can be applied to concentration maps from sources other than electrical tomography (e.g., CFD simulations of two-phase flows).

Keywords: electrical tomography, 3D visualisation of gas-liquid flow, bubble size and distribution, bubble mapping, flow regimes

*Corresponding author

Email address: m.wang@leeds.ac.uk (Mi Wang)

1. INTRODUCTION

Gas-liquid two-phase flow is a common phenomenon in industries, such as nuclear, pharmaceutical and gas-oil industries. The primary purpose of visualising flow in pipeline, in more general terms, is to understand flow dynamics for enhancing the process safety, production rate quality. Spatial and/or temporal distributions of gas and liquid phases in pipeline, i.e. flow regimes are crucial for design, analysis, and operation of two-phase flow systems [1]. The conventional methods to reveal the spatial distribution of gas in water is by applying an on-site inspection, i.e. observing bubbles within a physical boundary, through a transparent chamber, by a high-speed camera. This observation, however, is limited by the availability of such a transparent chamber and transparency of continuous phase in fluids. Moreover, the void fraction of gas phase also affects the reliability of the observation when it is beyond a certain threshold (e.g. 10% [2]). Therefore, alternative visualisation methods are highly demanded for an insightful understanding of gas-liquid flow.

Process tomography has been widely applied to measure and visualise multiphase flow in the past few decades. Particularly, electrical tomography is a type of visualisation techniques based on the phase difference in electrical properties, e.g. resistance or capacitance [3]. Compared with other tomographic techniques, electrical tomography, e.g. electrical resistance tomography (ERT) or electrical capacitance tomography (ECT), is capable of producing cross-sectional images with a relatively high temporal resolution (sub-millisecond) [4, 5, 6] but with a relatively low spatial resolution (up to 5%, i.e. the ratio of the smallest size of identifiable objects to the diameter of the used container) [7]. However, due 25 to the nature of the electrical field, electrical tomography is unable to produce homogeneous sensitivity distribution over its sensing domain [8]. It also suffers from ill-conditioned problems associated with its inverse solution and limited number of measurements. All these limitations together make electrical tomography incapable of producing tomograms with high spatial resolution with its current form. That is, they are unable to identify small bubbles below a certain size or to provide a clear interface between the dispersed phase and the continuous phase (e.g. gas and water). Nevertheless, despite its low spatial resolution, it has been reported, in terms of ERT, that it is capable of managing gas concentration close to 100% for a gas-water flow [8].

A common characteristic shared by the majority of advanced visualisation techniques is to present multiphase components in flows with scalar/vector identities, where the scalar usually refers to concentration, pressure, density, or mass, and the vector to velocity field. In simulations, scalar and vector data can be processed individually or integrally to reveal flow characteristics. For example, in computer visualisation and animation, the concentration and velocity fields are taken into account simultaneously to reconstruct bubbles in gas-water flow [9]. In contrast, experimental visualisation techniques, especially tomographic visualisation techniques, are generally limited only on concentration distribution. Although other methods can be applied to extract velocity, e.g. cross-correlation [10], the visualisation of velocity distribution is statistical rather than instantaneous. As a result, the majority of

tomography-based multiphase flow visualisation is built upon scalar data, e.g. concentration distribution, derived by the associated instruments.

Among the visualisation techniques for scalar fields, the method of colour mapping is the most widely applied, owing to its simplicity in computation and implementation [11]. The basic idea behind the colour mapping is to convert different scalar values to different colours according to a predefined lookup table. From visualisation and perception viewpoints, applying a lookup table should emphasise important characteristics, but reduce less important or irrelevant information to the minimum. Unfortunately, the colour mapping-based images by electrical tomography are unable to reveal sufficient flow characteristics, e.g. bubble size and distribution, owing to the limitations of electrical tomography [12, 13, 14]. In addition, the images are strongly affected by the definition of a lookup table, which may result in ambiguity for human and machine perception. For example, different images may represent same concentration distribution due to different definitions of lookup tables.

Another widely applied visualisation technique is surface extraction, or contouring in 2D. Basically, for a volume in a given scalar data (e.g. a stack of cross-sectional concentration tomograms), an isosurface is the connection of all points that have same isovalue [11]. That is, on the isosurface, the values of all points are constant. In the application to multiphase flow visualisation by tomographic techniques, surfaces represent the interfaces between each phase. For example, in [13], the 3D reconstructed tomograms as the input volumetric data were binarised by the given isovalue of 0.5, and the surface was retrieved, which represented the boundary between conductive and non-conductive phases. However, when applied to electrical tomograms, surface extraction is only able to identify the interfaces between large bubbles and the continuous phase. It tends to miss small bubbles, even when multiple isovalues are applied. This is primarily because of the small and gradual changed entailed by the reconstruction process of electrical tomograms.

In addition to commonly employed colour mapping and surface extraction, there are a few different approaches for the visualisation. In [2], wire-mesh sensor (WMS) was used for measuring bubble size and distribution in air-water flow in a vertical vessel, without the involvement of reconstruction process, i.e. on raw data. In Prasser's method, a bubble is reconstructed by firstly locating the centre of a bubble, and then swarming the neighbouring pixels around the centre to form the bubble. Obviously, the result may tend to be an overestimation of bubble size. When applying to electrical tomograms, this method is unable to identify small bubbles due to the relatively low spatial resolution of the tomograms. Another example is the application of raytracing technique by Manera [15], which works by tracing a path from an imaginary eye through each pixel in a virtual screen, and calculating the colour of the object visible through it [11]. Since bubbles in electrical tomograms are not clearly presented, the ray is unable to interact with individual objects, i.e. bubbles, and hence raytracing is not directly applicable to electrical tomograms. Ye et al. [16] applied conventional texture-based volume rendering technique in computer graphics to achieve real-time 3D visualisation on ECT tomograms, which essentially displays 3D volume

data in a 2D image by projection [11]. Again, this method does not manage to reflect adequate flow dynamics involving small bubbles.

In this paper, a novel approach is proposed to overcome the problems when using electrical tomography to visualise gas-liquid flow, which essentially 'reconstructs' bubbles based on concentration tomograms. For simplicity, it is assumed that gas bubbles are randomly distributed with a homogeneous volume fraction inside a small region, and the growth and collapse of the bubbles are trivial to be ignored [1]. According to the assumptions and the definition of gas volume fraction [1, 17], a new bubble-based lookup table can be defined to replace the lookup table in conventional colour mapping, in which bubble size relates to the average concentration of an unit, namely interrogation cell (IC), while its location is random inside the volume. With a carefully selected threshold, adjacent volumes are merged to form large bubbles. Those large bubbles are further processed using an enhanced isosurface algorithm to identify the boundaries between the large bubbles and the liquid. In the procedure, small bubbles are assumed to be spherical, whereas the shape of large bubbles is determined from input tomograms.

Compared to existing visualisation methods, our approach yields following advantages:

- It has the ability to manage a number of common flows including both horizontal and vertical pipeline layouts in industrial setups.
- Displaying bubbles instead of colours to reflect the spatial distribution of gas and liquid offers the opportunity to better understand the flow under investigation, such as visual recognition of flow regimes.
- The proposed approach is easily adapted to handle concentration distribution data, and therefore can be utilised as a generic model for other visualisation techniques.

The rest of the paper is arranged as follows. In Section 2, relevant background knowledge with regard to electrical tomography and typical flow regimes for vertical and horizontal pipeline flow is introduced. The detailed information about the approach is explained in Section 3, and the visualisation results are presented in Section 4. Then, conclusions are made in Section 5, along with a brief discussion of the benefits and limitations of the approach.

2. BACKGROUND

2.1. Electrical tomography

In general, electrical tomography measures the difference in electrical properties, e.g. permittivity for ECT and conductivity for ERT, of a multi-phase flow in a process vessel, by deploying one or more arrays of surface-mounted electrodes on the wall of the vessel, and then taking measurement and comparing these values with known reference values (namely, relative changes) to reconstructed relative property distribution. Current/voltage is injected into a pair of electrodes, meanwhile a set of

voltage responses are measured sequentially or synchronously on other electrode pairs. Based on the measurements, one frame of cross-sectional image can be reconstructed to represent the conductivity distribution, e.g. with a single-step linear back-projection (LBP) or advanced iterative algorithms [18, 13]. Since the focus of this paper is on the visualisation of gas-liquid flow using electrical tomography, the principle of the tomography will not be detailed here. The reader is referred to [3] for technical details of electrical tomography.

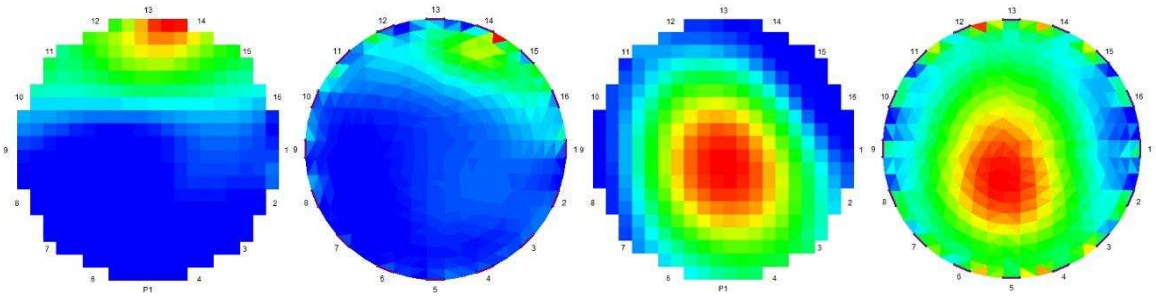

(a) (b) (c) (d)

Figure 1: ERT-based concentration tomograms of bubbly flow by (a) LBP and (b) SCG, and slug flow by (c) LBP and (d) SCG.

Due to the limitations of electrical tomography as mentioned previously, it is unable to identify small bubbles below a certain size or provide a clear interface between the gas phase and the continuous phase. Figure 1 shows examples of the impact of ERT limitations on visualisation. Figure 1a and Figure 1b are the concentration tomograms of bubbly flow in a horizontal pipe, by single-step LBP [19] and sensitivity theorem-based conjugate gradient reconstruction algorithm (SCG) [18] respectively, in which small and/or large bubbles exist at the top of the pipe, water at the bottom of the pipe. Figure 1c and Figure 1d are examples of concentration tomograms of slug flow in a vertical pipe, by the single-step LBP and iterative SCG respectively, in which slug bubble (large bubble) is at the centre, surrounded by water. Figure 1 clearly demonstrates that whether a simple LBP or an advanced reconstruction algorithm is applied, ERT struggles to locate small bubbles and show sharp edges between the phases. This problem also exists in ECT systems.

2.2. Typical flow regimes

A flow regime/pattern describes a specific spatial distribution (or topology) of gas and liquid phases in a given channel [1, 17]. Due to the complexity of the interaction between gas and liquid, as well as the impacts of physical and fluid properties, such as channel inclination, surface tension, an infinite number of flow structures could occur in a given channel. Fortunately, when a gas- liquid flow is in a steady

state, i.e. the flow with certain superficial velocity of each phase is fully developed, flow regimes can be simply categorised into a few different forms depending on pipe orientation [1, 17].

Four flow regimes in a vertical pipe and six flow regimes in a horizontal pipe were chosen to evaluate the proposed approach [20] in the following sections. Due to the scope of the research [20] and the limitations of electrical tomography, flow regimes to be targeted in the research did not cover all the regimes in the literature [1, 17]. Particularly, it was not attempted for applying the method for visualisation of mist and/or finely disperse bubble flow regimes in respect to horizontal and vertical flows.

2.2.1. Common flow regimes in a vertical pipe

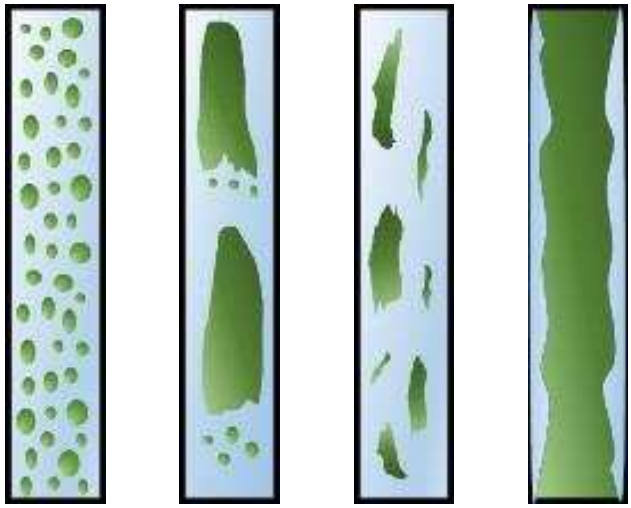

(a) (b) (c) (d)

Figure 2: Four typical flow regimes of gas-liquid upward flow in a vertical pipe. (a) bubbly flow; (b) slug flow; (c) churn flow; and (d) annular flow

In a vertical pipeline, there are four common flow patterns for fully-developed upward flow, including bubbly, slug, churn, and annular flow [1, 17], as depicted in Figure 2, in which the green is gas and the light blue is liquid. At a low gas volume fraction (a few percentage), gas ascends inside a pipe as dispersed bubbles, and bubble size is much less than the pipe diameter, and the distribution is homogeneous, as depicted in Figure 2a. When gas concentration increases to a certain level, dispersed bubbles coalesce to form large bullet-shaped bubbles (i.e. Taylor bubbles), with the diameter close to the pipe diameter, and is recognised as slug flow (Figure 2b). At still higher gas volume fractions, churn flow occurs, characterised by the deformation of Taylor bubbles to irregular and disordered bubbles, shown in Figure 2c. In this case, the flow is also called oscillatory flow, characterised by chaotic liquid movement in occasionally downward direction. Next, if gas volume fraction is very high, it continuously arises at the centre of the pipe, surrounded by a thin film of water on the pipe wall, as illustrated in Figure 2d.

2.2.2. Common flow regimes in a horizontal pipe

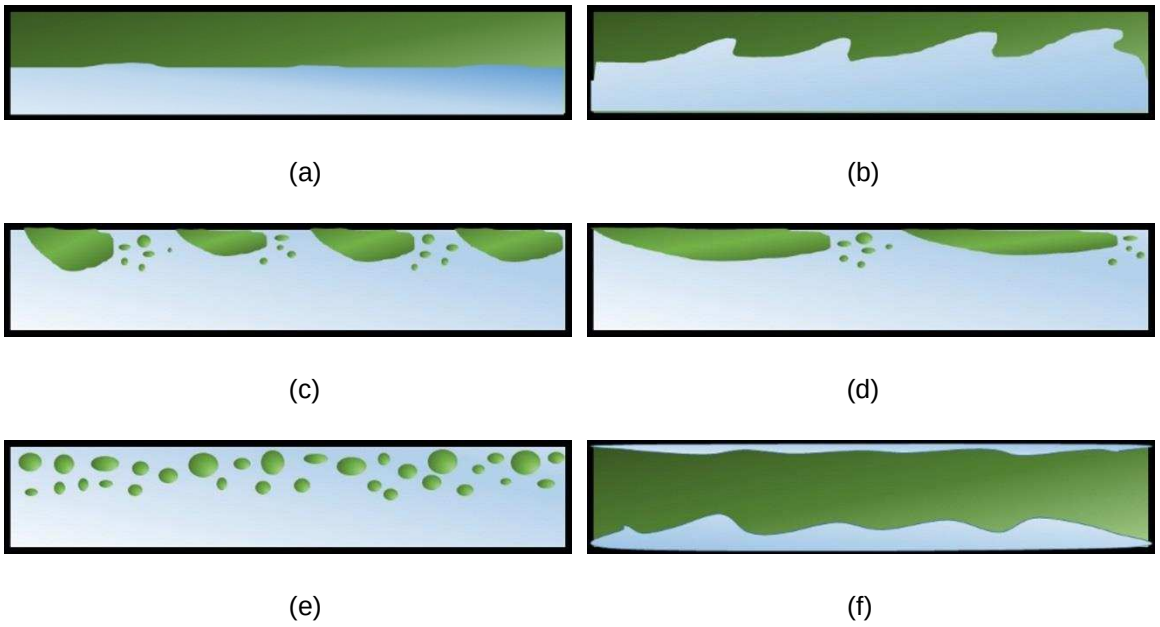

Figure 3: Six typical flow regimes of gas-liquid flow in a horizontal pipe. (a) stratified flow; (b) wavy stratified flow; (c) plug flow; (d) slug flow; (e) bubbly flow; and (f) annular flow.

At the same gas volume fractions, steady-state gas-liquid flow in a horizontal pipe produces different flow regimes comparing with those in a vertical pipe, due to the change of pipe orientation. Generally, there are six flow regimes that are commonly inspected [1, 17], as depicted in Figure 3. When gas and liquid velocities are low, the two phases are completely separated with a stable horizontal interface, where liquid goes to the bottom of the pipe and gas to the top (Figure 3a).

Increasing the velocities within a certain range results in the instability of the interface, on which waves are formed and travel. The dimensions of the waves depend on the relative velocity between the two phases, but without reaching the top of the pipe (Figure 3b). At lower gas velocity and higher liquid velocity, separated gas phase are deformed to large bubbles with the diameter smaller than the pipe diameter, located at the top of the pipe wall, and a thin film of liquid usually exists between the bubbles and the wall. This is called a plug flow (Figure 3c). Further increasing the gas volume fraction, slug flow occurs (Figure 3d), characterised by large amplitude waves at the interface of gas and liquid phases. The frequency of the waves, or the length of slug bubbles, depends on the relative velocity. When liquid velocity is high enough to fully disperse the gas phase, small bubbles are generated within the pipe and bubbly flow occurs. The closer the bubbles are to the bottom of the pipe, the smaller their diameters are, as shown Figure 3e. If increasing gas velocity to higher level, gas becomes continuous phase, positioning at the centre of the pipe and surrounding by a thin film of liquid, and the flow becomes annular flow (Figure 3f). Unlike the one in a vertical pipeline, the thickness of the liquid film in horizontal pipe is inhomogeneous, i.e. the film becomes thicker as closer to the bottom of the pipe.

3. THE APPROACH

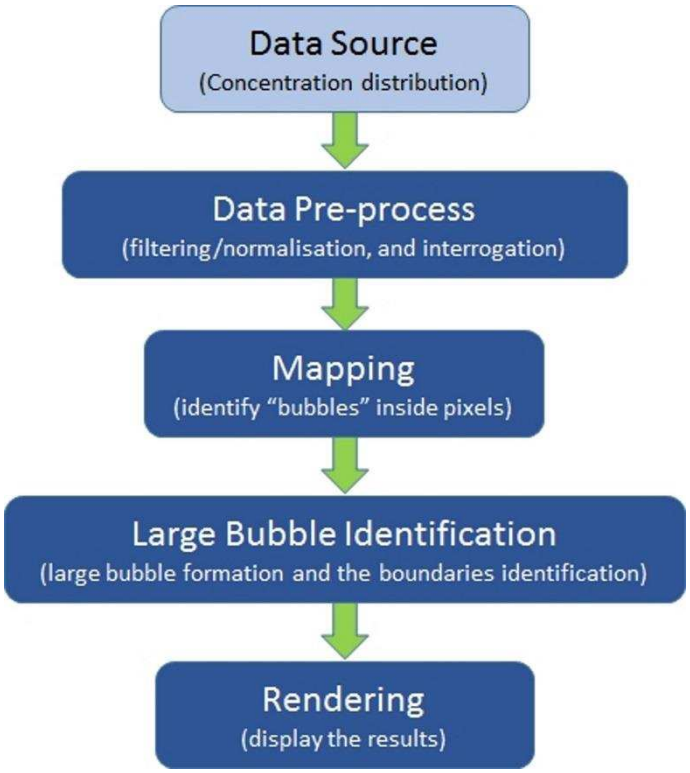

Figure 4: The pipeline of the new approach.

Conventionally, the colour of each pixel in electrical tomograms is determined by the corresponding concentration value of the pixel. For the convenience in discussion, the concentration value at the imaging pixel is defined as 0.0 or 1.0, corresponding to a pixel fully occupied by liquid or gas. Otherwise, the pixel concentration is within the range (0.0, 1.0), meaning the pixel is partially filled by gas. Following the same concept, a new lookup table can be established, in which a concentration value is transferred to a spherical bubble within a cell, and the value is maintained by the ratio of the areas of the spherical bubble against the cell. In order to reconstruct bubbles correctly, both spatial and temporal dimensional information have to be taken into account, by means of properly defining the dimension of interrogation cell (IC). Based on the dimensional definition of IC, the original concentration space is split into a coarser regular grid, to which a new lookup table is applied to reconstruct small bubbles, while indicating the rough locations of large bubbles. Afterwards, an enhanced isosurface algorithm is utilised to identify the boundary between large bubbles and liquid. Finally, when both small bubbles and large bubbles are generated, they are displayed by the common approach in computer graphics. Figure 4 shows the steps of the new approach, and each step will be addressed in the following sections.

3.1. Data pre-processing

Due to unavoidable noise during measurement, the converted concentration distribution may contain abnormal data, e.g. negative values. Therefore, it has to be filtered first. The filtered distribution is then split into IC by incorporating both spatial and temporal dimensional information into the definition of the cells. In particular, spatial information needs to consider the size of small bubbles in real situation, as well as the resolution capability of the systems, while temporal information needs to incorporate actual superficial velocity of gas phase and data acquisition speed of the employed systems into IC definition.

Given a scalar field $\varphi : \mathrm{R}^{\mathrm{d}} \rightarrow \mathrm{R}$, and a concentration set C over φ, concentration values are defined as:

$$\mathrm{C} = \{\mathrm{c_i}\}\, \mathrm{c_i} \in \mathrm{R} \tag{1}$$

The set C may need to be filtered/normalised to fit into meaningful range, i.e. [0.0, 1.0]. When the software [19] that was employed for the reconstruction process to generate stacked concentration tomograms provides a non-shifted mean concentration, the pixel concentrations are always within the range [0.0, 1.0] with some internal restrictions of the algorithm in the software, in which case filtering/normalisation is not required. Otherwise, a simple filter is defined by Equation 2:

$$\mathrm{F}\left(\mathrm{c_i}\right) = \begin{cases} 0.0 & \mathrm{c_i} < 0 \\ \mathrm{c_i} & 0 \le \mathrm{c_i} \le 1.0 \\ 1.0 & \mathrm{c_i} \ge 1.0 \end{cases} \tag{2}$$

When the filtering in the approach is required, a shift of averaged concentration with and without it may be introduced. However, the difference is actually too little to affect the quality of visualisation, and therefore the error is treated as ignorable.

The minimum size of an object that can be identified by electrical tomography is up to 5% of vessel size [7]. In other words, for a pipe with diameter D_p, the minimum size D_m is $D_m = 0.05D_p$. The spatial distinguishability is affected by many factors. When hardware is chosen and reconstruction algorithm selected, it is mainly affected by the size of pipe, because of the inhomogeneity of the sensitivity distribution, i.e. higher sensitivity at boundary area whereas lower sensitivity at central area, and the inverse relationship between distance and the strength of electrical field, i.e. the further the distance is, the weaker the field is. Consequently, larger pipe usually have a weaker sensitivity distribution than smaller size. Unfortunately, it is extremely difficult to sort out quantitative relationship between the minimum distinguish-ability and the affecting factors. In particular, when LBP is applied for reconstruction, bubbles with the size much less than the pipe diameter are all indistinguishable. On the other hand, when a gas-liquid flow is fully developed, bubble diameter is within the range of 5 mm to 20

mm regardless of vessel diameter [21, 22, 23, 24]. Accordingly, it is reasonable to assume that small bubbles are those with size below 20 mm, i.e. D_s = 20 mm. The spatial dimension of IC can therefore be defined as:

$$\mathrm{Dim}_s^{IC} = \left(\frac{D_s}{D_p / m} \right) * \left(\frac{D_s}{D_p / n} \right) \tag{3}$$

Where D_p is the diameter of the pipe containing the flow, m and n is the spatial grid definition of the original concentration set.

It is particularly noted that the third dimension of the input dataset only reflects temporal information (imaging speed), rather than spatial information. It therefore needs to be transferred to spatial information by incorporating local velocity of gas phase with the data acquisition speed of the tomography. Since the local velocity of gas phase was not measured during experiments, the superficial velocity of gas phase is therefore utilised here for the calculation. For instance, suppose the velocity of the gas phase is 1 m/s, and hardware collection speed is 1000 fps, if the measurement is taken for one second, the collected 1000 frames need to reflect the one-meter movement of the gas phase. That is, within the time for collecting two consecutive frames, i.e. 1/1000 = 1 ms, the flow actually moves forward 1 m/s * 1 ms = 1 mm. Therefore, the temporal dimension of IC can be defined as:

$$\mathrm{Dim}_t^{IC} = \frac{D_s}{v \Delta t} \tag{4}$$

Where v is the velocity of gas phase, and Δt is the temporal resolution of the original concentration set. Based on Equation 3 and Equation 4, original input of concentration distribution is split into a coarser grid by a number of IC, which will be further processed in next steps.

3.2. Mapping

In this step, a new lookup table is constructed, by which concentration values are transferred to bubbles that either partially or fully occupy an IC. That is, after this step, small bubbles are generated and the cores of large bubbles are identified. For gas-liquid flow, concentration of an IC is calculated as:

$$c_i^{IC} = \frac{\sum_{j=1}^{m} v_j^b}{v_i^{IC}} \tag{5}$$

Where c_i^{IC} is the gas mean concentration of the cell, v_i^b is the volume of ith bubble inside the given volume v_i^{IC}, and m is the number of bubbles inside the volume v_i^{IC}. In the context of gas-liquid flow, it

is acceptable to approximate that when an IC is reasonably small, there is only one bubble inside an IC, i.e. m is 1, thereby Equation 5 is rewritten to:

$$c_i^{IC} = \frac{v_i^b}{V_i^{IC}} \tag{6}$$

Equation 6 can be further rearranged to:

$$v_i^b = c_i^{IC} * v_i^{IC} \tag{7}$$

According to the dimension definition of IC, c_i^{IC} can be calculated by:

$$c_i^{IC} = \frac{1}{Dim_x^{IC} * Dim_y^{IC} * Dim_s^{IC}} \sum_{k=1}^{Dim_s^{IC}} \sum_{y=1}^{Dim_y^{IC}} \sum_{x=1}^{Dim_x^{IC}} c_{x,y}^k \tag{8}$$

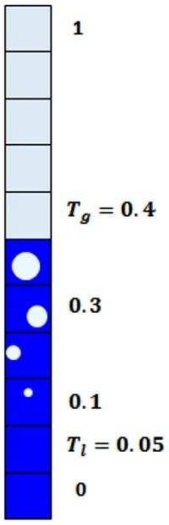

Figure 5: The new lookup table in 2D for bubble mapping.

According to Wang's investigation [25], the thresholding concentration for the transition from bubbly flow to turbulent flow in a static bubble column with a diameter of 5cm was around 40% [26]. Thereafter, as an approximated value in the paper, it is assumed when volume fraction of gas is above 40%, large bubbles appear. Therefore, 40% is used as the threshold value beyond which an IC is supposed to be fully occupied by gas. As another aspect, it is usually believed that there is a 5% measurement error owing to noise [7]. In other words, when the concentration is below 5%, it is assumed only one conductive phase in the pipeline, which in our case is the liquid phase. When the concentration is between 5% and 40%, there would be a small bubble inside IC, of which the size is determined by the

concentration. Incorporating those assumptions into Equation 8 as the transfer function to locate the entry of the new lookup table, and Equation 9 as the calculation of bubble radius within an IC, the new lookup table can be established, as depicted in Figure 5, in which T_g and T_l are the critical threshold values.

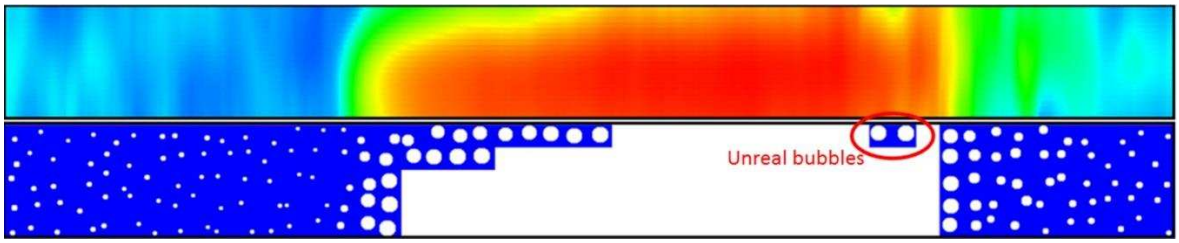

Figure 6: 2D stacked concentration tomograms by colour mapping and bubble mapping.

Once the bubble-based lookup table is built, it is ready to work on the interrogated concentration data. Figure 6 demonstrates an example of the application of conventional colour mapping and new bubble mapping to 2D stacked concentration distribution. In comparison to colour-based illustration, bubble-based one is able to reveal the size and position of small bubbles. As far as the large bubble in Figure 6 is concerned, the outline is already drawn, but inconsistent with the real-world situation in terms of bubble shape. This is because no consideration of merging neighbour bubbles beyond particular size has been taken. In addition, Figure 6 also illustrates the existence of some unreal bubbles in the red ellipse. In consequence, the next step is to merge neighbour bubbles to form larger bubbles.

3.3. Large bubble identification

After the mapping, some cells may be filled with small bubbles, instead of the boundary segments during the interrogation. Those neighbouring cells with high gas concentration should be merged together to form a large bubble.

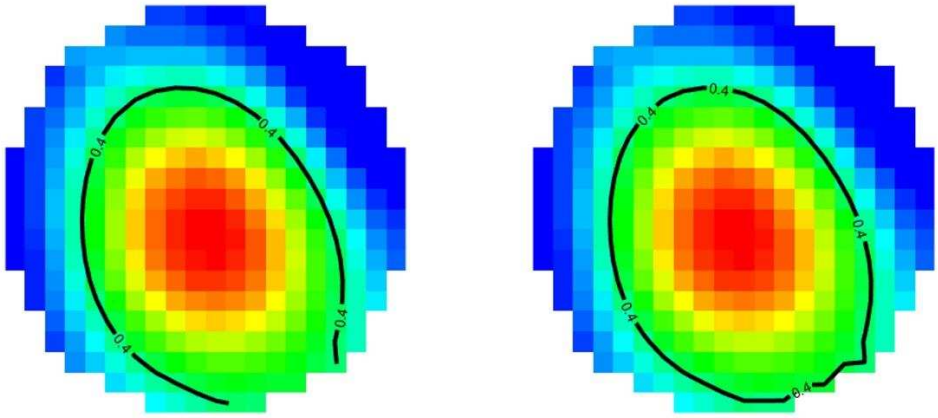

Figure 7: Identification of the boundary between a large bubble and liquid in an open contour (left), and a closed contour with a physical boundary (right).

After a cluster of the cells is located to form a large bubble, isofurface algorithm, e.g. Marching Cubes [27], is applied to extract the interface between the bubble and liquid. Suppose a cell with the values of all vertices are larger than a given threshold, but this cell is located at a physical boundary, e.g. pipe wall, the algorithm, unfortunately, will not respect that there should have an isosurface segment as the physical boundary. The left image in Figure 7 shows an example of an open contour, with a black contour of 0.4. It clearly demonstrates that without the consideration of the physical boundary, the contour becomes open, which is obviously inconsistent with reality. As a result, the algorithm has to be enhanced to reflect this situation. The right image in Figure 7 illustrates an example of the application of enhanced isosurface algorithm with the consideration of the physical boundary.

4. EVALUATION

The proposed approach is evaluated using concentration tomograms by ERT systems, on an industrial gas-liquid flow in both vertical and horizontal pipelines, covering the majority of the aforementioned flow regimes in Section 2.2[1]. For each flow regime, three images are presented by high-speed camera, by conventional colour mapping, and by the proposed approach. All colour mappings of concentration are generated same colour mapping (from blue to red) and same scale [0.0, 1.0]. Since the local velocity of gas phase was not measured, superficial velocity of gas phase is utilised here to calculate the temporal dimension of IC.

4.1. Gas-liquid flow in horizontal pipeline

Table 1: Gas superficial velocity and corresponding interrogation cell dimensions for horizontal flow

Gas superficial velocity (m/s)	Flow regimes	Spatial dimension of IC	Temporal dimension of IC	IC dimension
0.47	Stratified flow	4*4	0.0752	4*4*14
0.15	Bubbly flow	4*4	0.024	4*4*42
0.51	Plug flow	4*4	0.0816	4*4*13
2.06	Slug flow	4*4	0.3296	4*4*3
17.00	Annular flow	4*4	2.72	4*4*0.37

A set of experiments was conducted in a horizontal pipeline with diameter of 200 mm on the flow testing facilities at TUV NEL, and the data was gauged by a commercialised ERT system, namely V5R [5], at the speed of 312.5 dual frames per second (dfps). The mesh resolution of the 2D tomograms by V5R is 20*20. It is assumed that the diameter of small bubbles are less than 20 mm. The superficial velocity

[1] The results exclude churn ow, not for lack of applicability of the approach, but for lack of corresponding image/video.

of each phase is listed in Table 1. In consequence, spatial and temporal dimensions of the interrogation cell for each condition can be calculated according to Equation 3 and Equation 4. The results are listed in Table 1. The IC dimension in Table 1 means how the original concentration tomograms are split. For example, the IC dimension for stratified flow means the original 20*20 cross-sectional tomogram is divided into (20/4)*(20/4) = 5*5 coarser grid, and every 14 consecutive tomograms are averaged. Note that in Table 1, the temporal dimension of an IC for annular flow is less than 1, meaning the data has to be interpolated along the temporal axis. Another point is that the error by measuring pure liquid is less than 3% during the experiment. Consequently, 3%, instead of 5% is chosen for T_l.

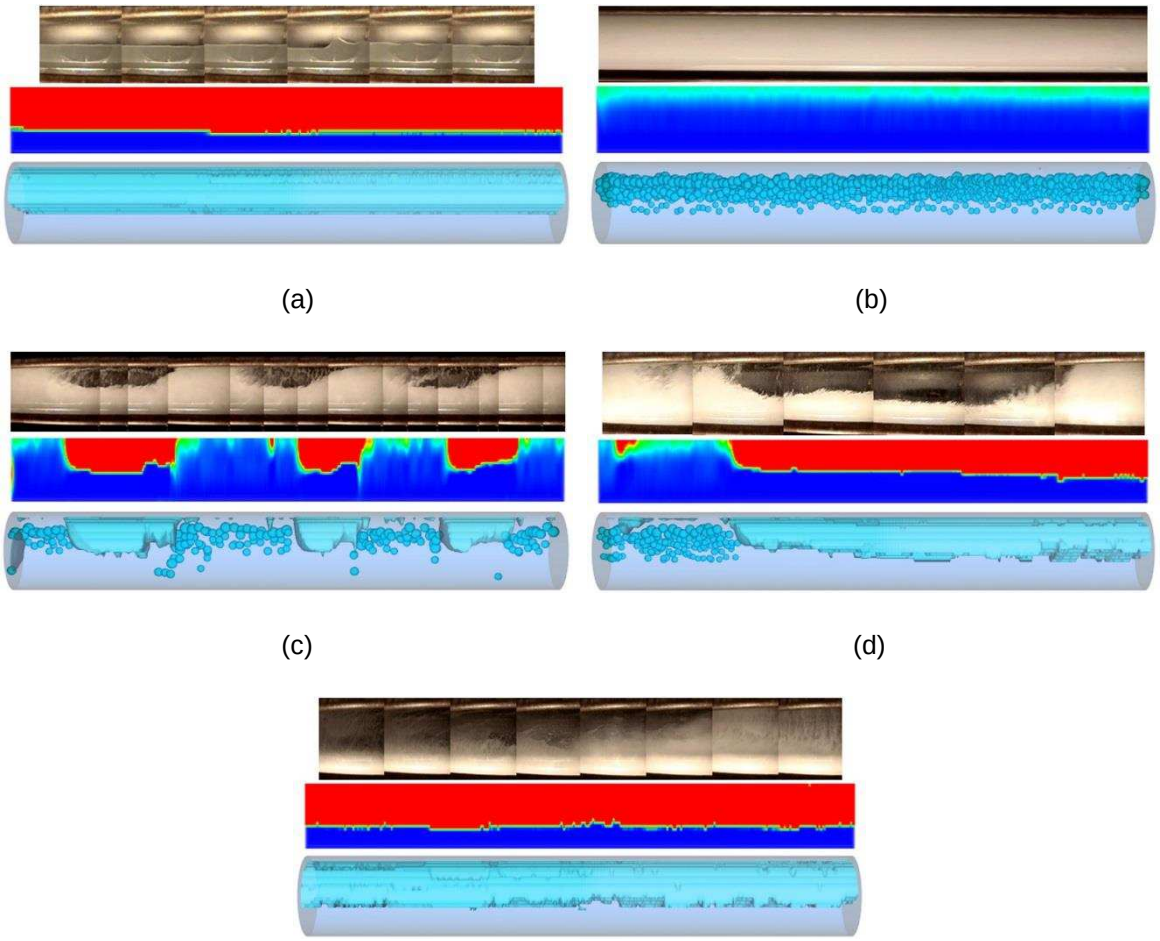

Figure 8: Visualisation of gas-liquid flow (flow direction from right to left) in a horizontal pipe by a high-speed camera, conventional colour mapping and proposed bubble mapping. (a) stratified flow; (b) bubble flow; (c) plug flow; (d) slug flow; and (e) annular flow.

Given the above parameters/thresholds, visualisation results based on the bubble mapping are depicted in Figure 8, along with the images from a high-speed camera taken through a photo chamber and the visualisation by conventional colour mapping. For a stratified flow in Figure 8a, the flow regime

can be clearly recognised by all images. The situation changes when coming to a bubbly flow as shown in Figure 8b. The images by the high-speed camera and the colour mapping are incapable of visualising the small bubbles in the bubbly flow, whereas the bubble mapping shows how the small bubbles distribute in the pipe. For a plug flow (Figure 8c) and a slug flow (Figure 8d), the camera and the colour mapping present similar results, i.e. the large bubbles can be located but the small bubbles are missing, whereas the bubble mapping complement the limitations by the methods. As far as annular flow is concerned, both the colour mapping and the bubble mapping are unable to demonstrate the thin water film at the top of the pipe. This is because the film is too thin to be identified by ERT system.

4.2. Gas-liquid flow in vertical pipeline

Table 2: Gas superficial velocity and corresponding interrogation cell dimensions for vertical flow

Gas superficial velocity (m/s)	Flow regimes	Spatial dimension of IC	Temporal dimension of IC	IC dimension
0.085	Bubbly flow	4*4	0.0085	4*4*118
0.51	Plug flow	4*4	0.051	4*4*20
18.424	Annular flow	4*4	1.8424	4*4*0.55

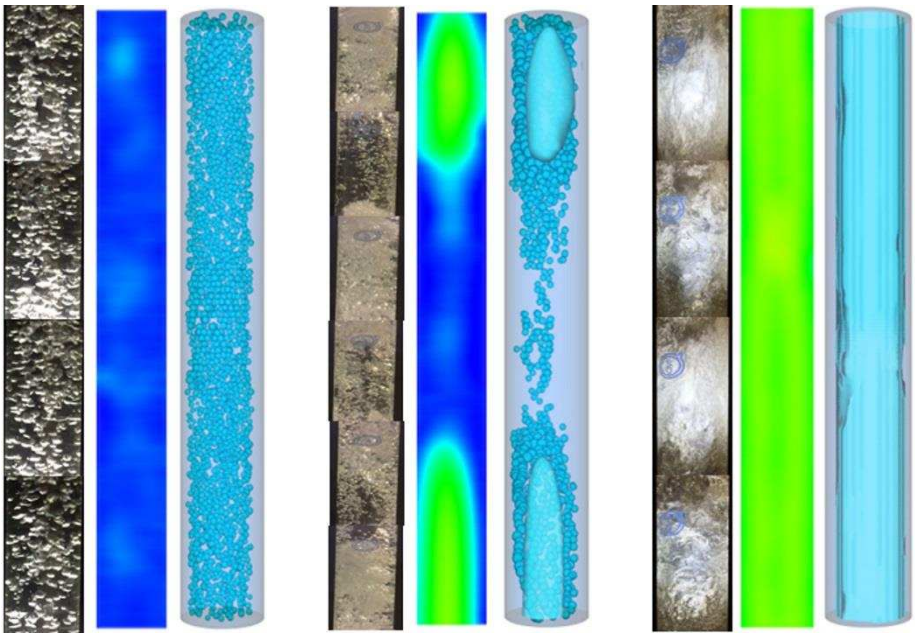

(a) (b) (c)

Figure 9: Visualisation of upward gas-liquid flow in a vertical pipe by a high-speed camera, conventional colour mapping and proposed bubble mapping. (a) bubbly flow; (b) slug flow; and (c) annular flow.

Another set of experiments was performed for upward gas-liquid flow in a 100 mm vertical section of the flow loop in the University of Leeds. 20*20 cross-sectional concentration data was obtained by another commercialised ERT system, called FICA [4], at the speed of 1000 dfps, and later stacked sequentially to form a 3D concentration dataset. The gas superficial velocity is listed in Table 2, as well as the cell dimensions in accordance with Equation 3 and Equation 4. 40% is used for T_g and 5% for T_l. The visualisation results, including bubbly flow, slug flow, and annular flow are presented in Figure 9, accompanied with concatenated images by high-speed camera and colour-based rendering.

The resultant visualisation of a bubbly flow in a vertical pipe is different from the one in a horizontal pipe, as depicted in Figure 8b and Figure 9a. In each group of images, e.g. Figure 8b, the top shows the photo from camera, the middle is the axial cross section of stacked tomograms, and the bottom shows the image produced by the bubble mapping approach. It is clearly demonstrated that both the camera and the bubble mapping can visualise the small bubbles, whereas the colour mapping does not. For a slug flow (Figure 9b), the flow regime can be recognized, but it is a little challenging to locate the exact size and distribution of the large bubbles due to the existence of small bubbles using the camera, whereas the stacked tomogram illustrates the approximate size and position of the large bubbles. In contrast, the bubble mapping reveals the small and the large bubbles. When it comes to an annular flow (Figure 9c), both the camera and the tomogram can show the flow regime, but struggle to reflect the thickness of the liquid film surrounding the gas, whereas the bubble mapping can.

4.3. Impact of the critical parameters

Since the parameters, i.e. T_g, T_l, and IC dimensions, are critical for the approach, the impact of the values on the results is evaluated. For each parameter, three different values are selected, and corresponding visualisation results are presented, while keeping the other parameters unchanged. Plug flow in horizontal pipeline (Figure 8c) is chosen for the demonstration because it contains both small and large bubbles.

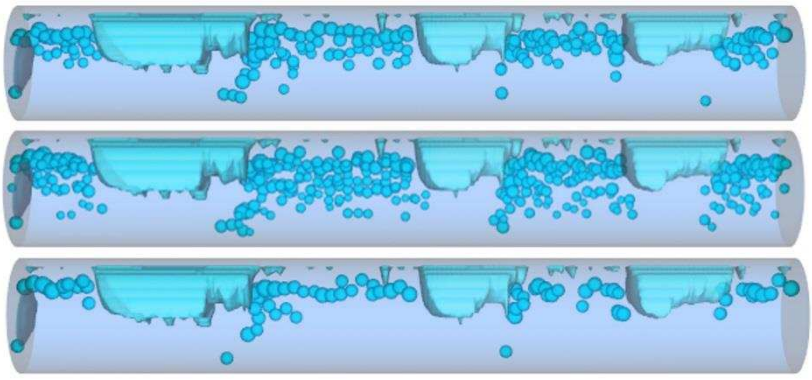

Figure 10: Visualisation results by different T_l of 0.05, 0.02, and 0.08 (from top to bottom).

Figure 10 depicts the influence of the threshold for pure liquid T_l on the visualisation. The original rendering with T_l = 0.05, i.e. the top one in the Figure, is set as the reference, and two more renderings with T_l = 0.02 (the middle one) and T_l = 0.08 (the bottom one) are generated. In the renderings, 174, 245, and 79 small bubbles are reconstructed, respectively, whereas the number of large bubbles is unchanged. In consequence, the threshold T_l affects the number of reconstructed small bubbles, but does not affect the large bubbles, mainly because the threshold determines the proportion of liquid phase. That is, the higher the threshold is, the less the liquid is, and in turn the more the gas is.

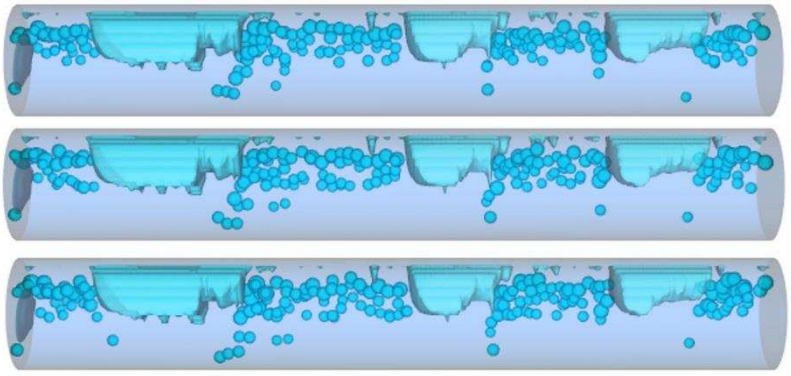

Figure 11: Visualisation results by different T_g of 0.4, 0.5, and 0.6 (from top to bottom).

The effect of the threshold T_g is presented in Figure 11, in which three different values, including 0.4, 0.5, and 0.6, are applied, and the outcomes are from top to bottom respectively. From visualisation point of view, the change does not have a distinguishable effect on the outcomes. The number of acknowledged small bubbles also proves it, in which there are 174, 174, and 183 small bubbles, respectively. Since Tg determines the full occupation of an IC by gas, it is crucial to the volume of large bubbles, and the boundaries between large bubbles and liquid, although the Figure does not explicitly illustrate it.

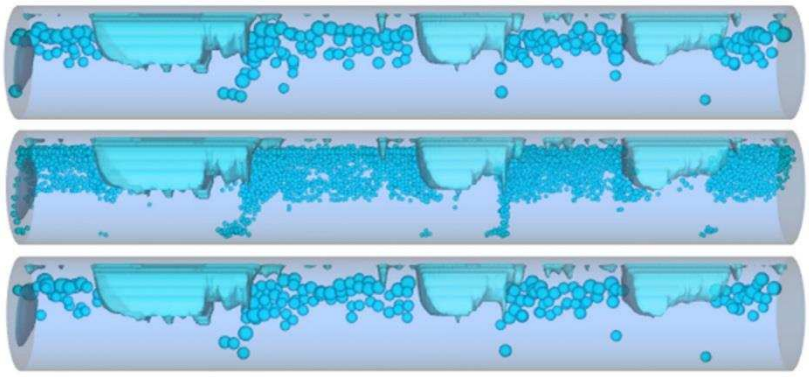

Figure 12: Visualisation results by different IC of 4*4, 2*2, and 5*5 (from top to bottom).

Another important parameter is the dimensional definition of IC, and Figure 12 shows the comparison. In essence, the size of IC is vital for the size of small bubbles, since the volume is not beyond an IC. In addition, it also influences the number of mapped small bubbles, since smaller IC results in more amount of IC with a given concentration distribution. Consequently, the smallest IC results in the bubbles of the smallest in size and the most in number, as shown by the middle one in Figure 12, in which totally 3251 small bubbles are located with the IC of 2*2 spatial dimension, compared to the ones by the IC of 4*4 and 5*5 with 174 and 158 small bubbles, respectively. In contrast, the appearance of large bubbles is irrelevant to the parameter.

5. CONCLUSION

A novel approach is proposed to visualise gas-liquid flow based on concentration distribution. The results have demonstrated that the approach is distinctly advantageous over the conventional concentration mapping using pseudo colours. With this approach, the spatial distribution of the gas phase is visualised as bubble, which conveys important flow information in a visually more straightforward manner than colour mapping of concentration can. With the assumptions that small bubbles uniformly and randomly reside in an IC, the visibility of those bubbles is enhanced to provide complementary flow information, while the gas concentration in the IC retains the same value as measured. For example, Figure 8b illustrates the bubbles in bubbly flow in horizontal tube tend to accumulate at the top of the pipe due to buoyancy, and moreover the closer the bubbles are to the top, the larger they become. In contrast, bubbles in vertical tube distribute more homogeneously, as depicted in Figure 9a.

Bubble mapping also provides more enlightening insights into flow dynamics, in contrast to colour mapping. For instance, in Figure 9c, it is challenging to identify flow regime from the colour-based result without additional information, whereas bubble-based result clearly and accurately presents the flow regime. This unambiguity, together with the binary format of the pixels in the results, i.e. a pixel is either in gas or in liquid, pave the way for computer-aided flow regime recognition using Boolean logic [28], of which the 2D variation is already applied for online flow regime recognition[2].

In comparison with other tomographic techniques (e.g. X-ray and WMS), electrical tomography probably has the lowest spatial resolution and therefore represents the most challenging case. If bubble mapping works in this case, it should be applicable to other (higher resolution and hence easier) cases.

However, there are still aspects for further improvement. The threshold values are critical to the results, and therefore have to be determined with extreme attention, which may need both empirical and theoretical evidence. The threshold for the evaluation is chosen as a global value, and therefore is

[2] The technical details will be presented in a separate paper.

applied to all cases. However, localised or case-specific thresholds may yield more accurate results, particularly when normalisation is applied during data pre-processing due to the re-scale of the data.

On the other hand, during the construction of the lookup table, it is presumed that an IC is full of gas when the corresponding concentration is above 40%, owing to the inability of the tomographic techniques to provide sharp interfaces between large bubbles and the liquid. This, unfortunately, no longer retains the mean concentration when large bubbles are involved. However, it does not have any negative effect on the identification and visualisation of flow regimes comparing the images by high-speed camera. In addition, this issue could be improved by applying advanced algorithms in both tomography and computer graphics, such as the one in the literature [18] and [29], respectively. However, it was understandable that ERT may produce a considerable underestimation error from imaging of large non-conductive object.

It should also be noted that the information on gas phase local velocity is necessary if the visualisation in both the temporal and spatial dimensions of IC is required, which can be achieved by applying the cross correlation method to a data set acquired from a dual sensing planes with a sufficient speed, such as the on in [30]. In addition, it is difficult to apply the method for visualisation of mist and/or finely disperse bubble flow regimes in respect to horizontal and vertical flows since these flow regimes present little variation in either permittivity or conductivity.

ACKNOWLEDGEMENT

This work is funded by the Engineering and Physical Sciences Research Council (EP/H023054/1, IAA (ID101204)) and the European Metrology Research Programme (EMRP) project Multiphase flow metrology in the Oil and Gas production, which is jointly funded by the European Commission and participating countries within Euramet and the European Union.

REFERENCES

[1] C. E. Brennen, Fundamentals of Multiphase Flows, Cambridge University Press, 2005.

[2] H.-M. Prasser, D. Scholz, C. Zippe, Bubble size measurement using wire-mesh sensors, Flow Measurement and Instrumentation 12 (4) (2001) 299-312.

[3] M. Wang (Ed.), Industrial Tomography Systems and Applications, Woodhead Publishing, 2015.

[4] M. Wang, Y. Ma, N. Holliday, Y. Dai, R. Williams, G. Lucas, A high-performance EIT system, Sensors Journal, IEEE 5 (2) (2005) 289-299.

[5] J. Jia, H. I. S. M. Wang, H. Li, A novel tomographic sensing system for high electrically conductive multiphase flow measurement, Flow Measurement and Instrumentation 21 (3) (2010) 184-190, special Issue: Validation and Data Fusion for Process Tomographic Flow Measurements.

[6] Z. Cui, H. Wang, Z. Chen, Y. Xu, W. Yang, A high-performance digital system for electrical capacitance tomography, Measurement Science and Technology 22 (5) (2011) 055503.

[7] M. Wang, F. J. Dickin, R. Mann, Electrical resistance tomography sensing systems for industrial applications, Chemical Engineering Communications 175 (1) (1999) 49-70.

[8] J. Jia, M. Wang, Y. Faraj, Evaluation of eit systems and algorithms for handling full void fraction range in two-phase flow measurement, Measurement Science and Technology 26 (1) (2015) 015305.

[9] J. Tan, X. Yang, Physically-based fluid animation: A survey, Science in China Series F: Information Sciences 52 (5) (2009) 723-740.

[10] M. Beck, A. Plaskowski, Cross Correlation Flowmeters, Their Design and Application, Taylor & Francis, 1987.

[11] C. Hansen, C. Johnson, Visualization Handbook, Elsevier Science, 2011.

[12] R. Banasiak, R.Wajman, T. Jaworski, P. Fiderek, H. Fidos, J. Nowakowski, D. Sankowski, Study on two-phase flow regime visualization and identification using 3d electrical capacitance tomography and fuzzy-logic classification, International Journal of Multiphase Flow 58 (2014) 1- 14.

[13] K. Wei, C. Qiu, M. Soleimani, K. Primrose, ITS reconstruction tool-suite: An inverse algorithm package for industrial process tomography, Flow Measurement and Instrumentation 46, Part B (2015) 292-302, special issue on Tomography Measurement & Modelling of Multiphase Flows.

[14] M. Wang, Q. Wang, B. Karki, Arts of electrical impedance tomographic sensing, Phil. Trans. R. Soc. A 374 (2070) (2016) 20150329.

[15] Manera, H.-M. Prasser, D. Lucas, T. van der Hagen, Three-dimensional flow pattern visualization and bubble size distributions in stationary and transient upward flashing flow, International Journal of Multiphase Flow 32 (8) (2006) 996-1016.

[16] L. Ye, W. Yang, Real-time 3d visualisation in electrical capacitance tomography, in: Imaging Systems and Techniques (IST), 2012 IEEE International Conference on, 2012, pp. 40-44.

[17] S. Corneliussen, J.-P. Couput, E. Dahl, E. Dykesteen, K.-E. Frysa, E. Malde, H. Moestue, P. O. Moksnes, H. T. Lex Scheers, Handbook of multiphase flow metering (2005). URL http://nfogm.no/wp-content/uploads/2014/02/MPFM_Handbook_Revision2_2005_ISBN-82-91341-89-3.pdf

[18] M. Wang, Inverse solutions for electrical impedance tomography based on conjugate gradients methods, Measurement Science and Technology 13 (1) (2002) 101.

[19] Industrial Tomography Systems Plc., Speakers House, 39 Deansgate, Manchester M3 2BA, ITS System 2000 Version 7.0 p2+ Electrical Resistance Tomography System - Users Manual (Nov. 2009).

[20] D. Millington, Eng58 multiphase flow metrology in oil and gas production - work package 4 (flow visualisation), Tech. rep., TUV NEL (2016).

[21] R. O. S. Guet, G. Ooms, Inuence of bubble size on the transition from low-re bubbly flow to slug flow in a vertical pipe, Experimental Thermal and Fluid Science 26 (6-7) (2002) 635-641.

[22] R. S. Sanders, M. M. Razzaque, J. Schaan, K. Nandakumar, J. H. Masliyah,A. Afacan, S. Liu, Bubble size distributions for dispersed air-water flows in a 100 mm horizontal pipeline, The Canadian Journal of Chemical Engineering 82 (4) (2004) 858-864.

[23] H. Jin, M. Wang, R. Williams, Analysis of bubble behaviours in bubble columns using electrical resistance tomography, Chemical Engineering Journal 130 (23) (2007) 179-185, special Issue for the 4th World Congress on Industrial Process TomographySpecial Issue - Industrial Process Tomography.

[24] F. Qi, G. Yeoh, S. Cheung, J. Tu, E. Krepper, D. Lucas, Classification of bubbles in vertical gas-liquid flow: Part 1 an analysis of experimental data, International Journal of Multiphase Flow 39 (2012) 121- 134.

[25] M. Wang, X. Jia, M. Bennett, R. A. Williams, Flow regime identification and optimum interfacial area control of bubble columns using electrical impedance imaging, in: 2nd World Congress on Industrial Process Tomography, 2001, pp. 726-734.

[26] W.-D. Deckwer, Bubble column reactors, John Wiley and Sons Ltd, 1992.

[27] W. E. Lorensen, H. E. Cline, Marching cubes: A high resolution 3d surface construction algorithm, SIGGRAPH Comput. Graph. 21 (4) (1987) 163-169.

[28] N. P. Ramskill, M.Wang, Boolean logic analysis for flow regime recognition of gas-liquid horizontal flow, Measurement Science and Technology 22 (10) (2011) 104016.

[29] J. C. Anderson, C. Garth, M. A. Duchaineau, K. I. Joy, Smooth, volume-accurate material interface reconstruction, IEEE Transactions on Visualization and Computer Graphics 16 (5) (2010) 802-814.

[30] H. Li, M. Wang, Y.-X. Wu, G. Lucas, Volume flow rate measurement in vertical oil-in-water pipe flow using electrical impedance tomography and a local probe, Multiphase Science and Technology 21 (1-2) (2009) 81-93.